Insect Biochemistry and Molecular Biology 113 (2019) 103207

Contents lists available at ScienceDirect

Insect Biochemistry and Molecular Biology

journal homepage: www.elsevier.com/locate/ibmb

Structural and functional differentiation of a fat body-like tissue adhering to testis follicles facilitates spermatogenesis in locusts

Dani Ren[a,1], Wei Guo[a,1], Pengcheng Yang[b,1], Juan Song[a,c], Jing He[a], Lianfeng Zhao[b,c], Le Kang[a,b,c,*]

[a] State Key Laboratory of Integrated Management of Pest Insects and Rodents, Institute of Zoology, Chinese Academy of Sciences, Beijing, China
[b] Beijing Institute of Life Science, Chinese Academy of Sciences, Beijing, China
[c] University of Chinese Academy of Sciences, Beijing, China

ARTICLE INFO

Keywords:
Transcriptome
Mitotic/endocycle switch
Cell cycle
Regional differentiation
Zinc-finger transcriptional factor

ABSTRACT

The fat body is distributed throughout the body of insects, playing the essential role in intermediary metabolism and nutrient storage. However, the function of differentiation of fat bodies adhering to different tissues remains largely unknown. Here, we identified a fat body-like tissue (FLT) surrounding testis follicles and described its features at morphological, cellular and molecular levels. The FLT is morphologically distinguished with the abdominal fat body (FB) and dominated by diploid cells instead of polyploid cells. The transcriptomic analysis demonstrated that the FLT and FB have dramatically different gene expression profiles. Moreover, genes in the cell cycle pathway, which include both DNA replication- and cell division-related genes, were successively active during development of the FLT, suggesting that FLT cells possibly undergo a mitotic cycle rather than an endocycle. Deprivation of the FLT resulted in distortion of the testis follicles, disappearance of sperm bundles, reduction of total sperm number and increase of dead sperm, indicating a critical role of the FLT in the spermatogenesis in testis follicles. The special functional differentiation of the two similar tissues suggested that FLT-FB cells are able to establish a promising system to study mitotic-to-endocycle transition.

1. Introduction

The fat body, a unique tissue to insects, is functionally equivalent to the mammalian liver and adipose tissue (Arrese and Soulages, 2010). Unlike the solid structure of the liver, the fat body in insects is a loose tissue irregularly distributed throughout the hemocoel, preferentially attached to the tegument or surrounding other tissues (Arrese and Soulages, 2010; de Oliveira and da Cruz-Landim, 2003). So, its consistence was given by the trachea and the amorphous components of the connective tissues (de Oliveira and da Cruz-Landim, 2003). Fat bodies rarely present adhesive and communication junctions and appear as a mass of cells organized in one or two cells thickness layers or as small granules suspended in the hemocoel (de Oliveira and da Cruz-Landim, 2003). Based on the distributed regions or attached tissue types, fat bodies displayed regional differentiation in metabolic and cytological features (Arrese and Soulages, 2010; Haunerland, 1995). In the fruit fly *Drosophila melanogaster*, more protein granules were found in fat body cells of posterior segments of the larvae (Tysell and Butterworth, 1978) and the kynurenine is synthesized only in the anterior part (Dortland and Esch, 1979; Rizki and Rizki, 1972). In the Colorado potato beetle *Leptillotarsa decemlilleata*, the peripheral fat body contains more glycogen than the perivisceral tissue (Dortland and Esch, 1979). Moreover, the peripheral fat body in the silkworm *Bombyx mori* is predominantly responsible for biosynthetic activity, while the perivisceral fat body is differentiated as a storage tissue (Vanishree et al., 2005). In the cotton bollworm *Heliotis zea*, the red hairy caterpillar *Amsacta albistriga* and the midge *Chironomus thummi*, the peripheral fat body was the site of the most active protein synthesis (Chandrasekar et al., 2008; Haunerland, 1995). In spite of these reports on regional and functional differentiation of insect fat bodies, the detailed cytological characteristics in cell ploidy and changes in gene expression associated with special functions are largely unknown.

Polyploidy plays critical roles in the regulation of cell expansion and/or cell differentiation to achieve tissue growth (Bramsiepe et al., 2010; Inze and De Veylder, 2006; Lilly and Duronio, 2005). During the embryogenesis of fruit fly, fat body cells display the transition to polyteny (Smith and Orr-Weaver, 1991). Our previous studies found that fat body cells in the migratory locust are polyploidy by undergoing

* Corresponding author. Institute of Zoology, Chinese Academy of Sciences, 1 Beichen West Road, Chaoyang District, Beijing, 100101, China.
E-mail address: lkang@ioz.ac.cn (L. Kang).
[1] These authors contribute equally to this paper.

https://doi.org/10.1016/j.ibmb.2019.103207
Received 20 February 2019; Received in revised form 27 July 2019; Accepted 28 July 2019
Available online 14 August 2019
0965-1748/

a modified mitotic cycle called endocycle during adult stages (Guo et al., 2014; Wu et al., 2016, 2018). During the mitotic cycle, cells pass through G1–S–G2 phases to duplicate their DNA followed by M phase to partition the genetic material and divide the mother cell into two daughter cells. However, during the endocycle, cells increase their genomic DNA content by successive DNA replication without division. Generally, our studies show that polyploidization is generated in tissues with highly active biosynthesis, which massively produce particular proteins to support their biological functions (Guo et al., 2014; Wu et al., 2016, 2018). The key question in endocycle regulation is how the transition from the mitotic phase to the endocycle is controlled (Jordan et al., 2006). Because the mechanism of mitotic to endocycle switch (MES) varies in different cell types and the regulators were developmentally programmed, thus it is difficult to identify the directly machinery action on the mitotic/endocycle switch (Deng et al., 2001; Ishida et al., 2009; Lilly and Duronio, 2005).

The migratory locust *Locusta migratoria*, an insect model system of incomplete metamorphosis, is reproductive in high fecundity, which depends on the absorption of nutrients secreted from its fat bodies. In female locusts, the fat body is a tissue closely related to oogenesis and egg production, and undergoes endocycle during development post adult eclosion (Guo et al., 2014, 2019; Wu et al., 2016, 2018). In male locusts, besides the fat body in the abdomen, there are also large amounts of fat cells surrounding 150–200 testis follicles (Szollosi and Marcaillou, 1977, 1979), named the fat body-like tissue (FLT). In the present study, we firstly confirmed that the FLT shares mutual characteristics with the FB, indicating that the FLT is a fat body-like tissue. Furthermore, we characterized the differences between the FB and FLT in morphology and cytology. Respective marker genes between these two tissues were identified by PCA analysis based on transcriptomic data of the FB and FLT. Bioinformatic and functional validation indicated that the FLT is regionally specialized tissue that undergoes active mitotic cycle, and plays important role in spermatogenesis in testis follicles.

2. Material and methods

2.1. Insects rearing

The migratory locust colonies were reared in the gregarious phase under a photoperiod of 14 h light: 10 h dark at 30 ± 2 °C as previously described (Ren et al., 2014). The diet included the continuously supplied wheat bran together with fresh wheat seedlings provided once daily. Adult male locusts were used in the experiments.

2.2. Tissue imaging and confocal microscopy

The anatomical photo was taken by a Canon EOS550D camera. Images of the FB and FLT were captured with the Leica M205C microscope. Tissues were fixed in the 4% paraformaldehyde in PBS for 20 min and permeabilized with 0.3% Triton X-100 for 30 min at room temperature. For F-actin and nuclei staining, tissues were incubated with 0.2 U/μl Phalloidin-Alexa Fluor 488 (Invitrogen) plus 1% bovine serum albumin in phosphate-buffered saline (PBS) for 30 min and 5 mM Hoechst 33342 (Sigma-Aldrich) in PBS for 10min, sequentially. For lipid droplet staining, tissues were incubated with Nile red (Invitrogen) for 10 min at room temperature. Images were captured by ZEISS LSM 710 confocal laser scanning microscopy and processed with ZEN2010 software.

2.3. Triglyceride measurement

Triglyceride in the tissues were measured using Tissue Triglyceride Assay Kit (Applygen Technologies) following the manufacture's instruction. Briefly, tissues were dissected and washed 3 times in PBS, and then homogenized in extraction buffer and incubated at 70 °C for 15 min. The supernatant was collected for triglyceride measurement after centrifugation. The absorption of samples was determined by a VERSAmax Tunable Microplate Reader.

2.4. Flow cytometry

The FB, FLT and brain were homogenized in a Dounce homogenizer, respectively. The sperm bundle was collected from the seminal vesicles and digested by 1.25% trypsin. Cells were collected by centrifugation (800 g) and fixed in 70% ethanol overnight, followed by incubated in PBS buffer containing 100 mg/ml RNaseA (Promega), 50 mg/ml propidium iodide (Sigma) and 0.2% Triton X-100 for 2 h at 4 °C. Cells were analyzed post filtration with a 300-mesh cell strainer (BD Falcon) using a BD FACS Calibur Flow Cytometry System with Flowjo 7.6.1 software (BD Biosciences).

2.5. Transcriptomic sequencing and data processing

The FB or FLT of 3 adult male locusts were collected and pooled together respectively as one biological replicate. Two biological replicates were sampled for RNA-seq at 0, 4 and 8 days post adult eclosion, respectively. Total RNA was extracted using TRIzol reagent (Invitrogen, Carlsbad, CA, USA) according to the manufacturer's instructions. Approximately 3 μg total RNA was used to establish a paired-end RNA-seq library for transcriptome sequencing on an Illumina HiSeq 2000 sequencer (Illumina, San Diego, CA, USA). After the low-quality reads had been trimmed and the adapters had been removed, the clean RNA-seq reads were mapped to the reference genome using Tophat2 (version 2.0.13) with default parameters (Kim et al., 2013). The genome sequence and gene structure annotation data of *Locusta migratoria* were downloaded from http://www.locustmine.org/download.htm (Yang et al., 2019). The unique mapped reads were used to calculate the number of reads that mapped to every gene model using HTSeq (Anders et al., 2015). The influence of differences in RNA output size between samples was reduced by trimmed mean of M-values (TMM) method (Robinson and Oshlack, 2010). Gene expression level was measured as reads per kilobase per million reads (RPKM). Principal component analysis (PCA) was accomplished using the princomp and pca functions. Student's *t*-test was used for significance test between FLT and FB at PAE0, 4 and 8, respectively. Analysis of variance (anova function in R environment) was used for significance test among FLT or FB groups during adult maturation. Genes with significance levels of $P < 0.05$ and fold change ≥ 1.5 were considered as differentially expressed. Cluster analysis was performed using average linkage method with spearman correlation as distance in Gene Cluster 3.0 software. Java treeview software (version 1.1.1) was used for visualization. As we previously used (Wang et al., 2014), enrichment analysis of Kyoto Encyclopedia of Genes and Genomes (KEGG), Gene ontology (GO) and Interpro (IPR) for the DEGs was carried out based on an algorithm presented by GOstat (Beissbarth and Speed, 2004), with the whole annotated gene set as the background. The P-value was approximated using the chi-square test. Fisher's exact test was used when any expected value of count was below 5.

2.6. qRT-PCR

First-strand cDNA was reverse-transcribed from 2 μg of total RNA using FastQuant RT Kit with gDNase (Tiangen, Beijing, China) following the manufacturer's instructions. qRT-PCR was performed on Roche LightCycler 480 (Roche, Mannheim, Germany) using SuperReal PreMix Plus (SYBR Green) Kit (Tiangen, Beijing, China), initiated at 95 °C for 2 min, then 40 cycles at 95 °C for 20 s followed by 58 °C for 20 s and 68 °C for 1 min with locust Ribosomal protein 49 (Rp49) as the internal control. The 2-ΔΔCt method was used to calculate the relative expression levels. Primers for qRT-PCR are listed in Table S1.

2.7. FLT-deprivation operation

The septum between the first and the second segment was cut open by scissors in locusts within 12 h post adult eclosion. The testes were pulled out to deprive the FLT from about 1/3 of total testis follicles and put back after operation. The locusts were sacrificed after 8 days post operation for Tsl observation and 10 days post operation for estimate of sperm number and viability. Locusts and surgical instruments were sterilized by 75% ethanol before and after operation.

2.8. Estimate of sperm number and viability

The paired seminal vesicles from each male were put into 100 μl of SFX-Insect cell culture media (GE Healthcare HyClone) and opened with forceps. Then, 140 μl 1.25% trypsin was added and gently stirred to disperse the sperm bundle for 2 min. The suspension was pipetted to calculate the sperm number by hemocytometer. The experimental procedure for estimating sperm viability is according to Damiens et al. (2002) with modification. Six 3 μL drops of the suspension were deposited on clean slides. Sperm samples collected from males were treated with SYBR 14: propidium iodide (LIVE/DEAD Sperm Viability Kit, Thermo Fisher Scientific, Waltham, MA USA) as follows: 0.5 μL of 50-fold diluted SYBR 14 dye were added to sperm samples on the microscope slide. The preparation was gently stirred and incubated at 28 °C for 5min, and then 0.5 μL of propidium iodide solution was added and incubated at 28 °C for 5min. Images were captured by fluorescence microscopy (Leica, DM2500, Leica Microsystems). The percentage of red or green subpopulations of sperm were determined in each drop. SYBR 14 labels live sperm with green fluorescence and propidium iodide labels dead sperm with red fluorescence.

2.9. Data analysis

Data were analyzed using the IBM SPSS Statistics v.19 software (SPSS Inc., Chicago, IL). Differences between treatments were compared either by Student's t-test or by one-way analysis of variance (ANOVA). Differences were considered significant at $P < 0.05$. Values are reported as mean ± SE.

3. Results

3.1. Localization of a specialized fat body-like tissue around testis follicles

In the hemocoel of male locusts, the abdominal fat body (FB) appears yellow and attaches to variant tissues including the cuticle, muscle, gut, and testes (Fig. 1A and B). After testes were dissected and the attached FB was cleanly separated, testes still appear yellow. Further dissection showed testes composed of hundreds of testis follicles (Tsl) wrapped by the adhesive fat body-like tissue (FLT) (Fig. 1C).

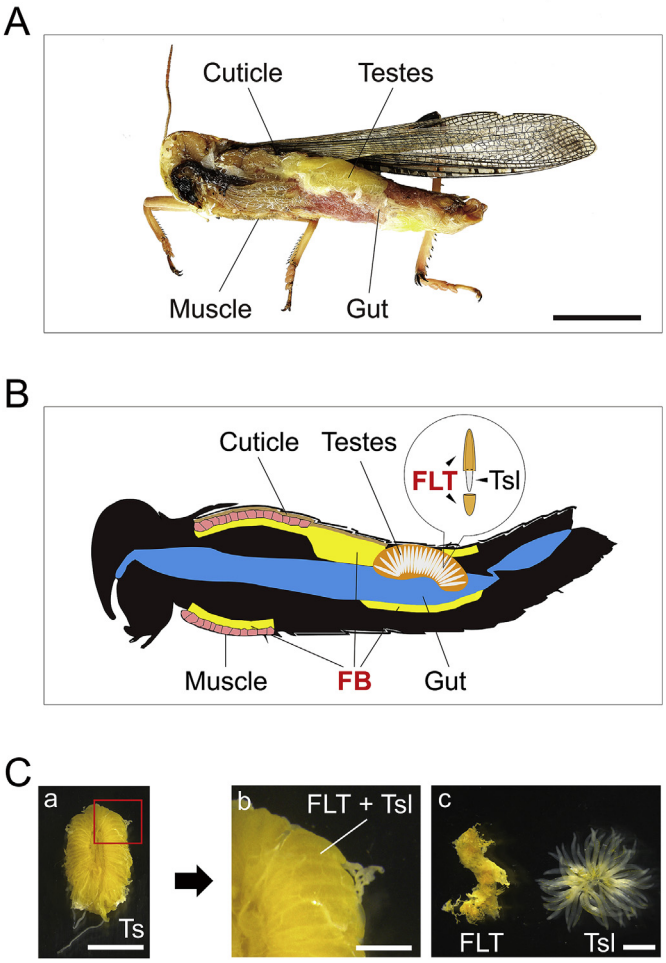

Fig. 1. Localization of the abdominal fat body (FB) and the fat body-like tissue (FLT) in male locusts at 8 days post adult eclosion (PAE8). (A) Image of the distribution of the FB or FLT around other tissues. Scale bar, 1 cm. (B) Diagram of the distribution of the FB or FLT around other tissues. (C) The anatomic structure of the testis (Ts). Tsl, testis follicles. Scale bars: a, 5 mm; b, 500 μm; c, 2 mm.

3.2. Mutual characteristics shared between the FB and FLT

Lipid is the major component of the fat body, representing more than 50% of the dry weight (Arrese and Soulages, 2010). We stained lipid droplets in the FB, FLT, brain (Br) and testis follicles (Tsl) to evaluate the lipid accumulation. Like in the FB, numerous lipid droplets were preserved in the FLT. However, few lipid droplets were observed in the Br and Tsl (include germinative area and zone of transformation) (Fig. 2A). Negative control of lipid droplets staining in the FB, FLT, Br and Tsl displayed no red fluorescent signals (Fig. S1). We further measured the titers of triglyceride in the FB, FLT, Br and Tsl. The FB and FLT displayed no significant difference on relative triglyceride level. However, the relative triglyceride level in the FB and FLT displayed 2.8-fold and 3.1-fold higher than in the Br respectively, and 4.8-fold and 5.4-fold higher than in the Tsl respectively (Fig. 2B).

Polyploidy is a dramatic characteristic of fat body cells (Guo et al., 2014; Li et al., 2019; Wu et al., 2016, 2018). Cell ploidy analysis by flow cytometry showed that both the FB and FLT had 2C, 4C and 8C populations. However, the brain and sperm had only 2C and C population, respectively (Fig. 2C).

In order to detect whether the FLT share the general functions with the FB, we selected 16 reported genes related to nutrient storage (Hex1, Hex4), energy metabolism (ApoIII, BBOX1, Lsd1, Lsd2, Tret1), innate immunity (GNBP3, PGRP, Toll), detoxification (FMO, GST) and other functions (HP19, PMP-D2, Tf, JHBP) (Arrese and Soulages, 2010; Boigegrain et al., 1992; Levy et al., 2004; Li et al., 2019; Palm et al., 2012; Wang et al., 2013). The qRT-PCR results in 9 tissues including the FB, FLT, Tsl, Sv (seminal vesicle), Mg (midgut), He (hemolymph), An (antenna), Tg (thoracic ganglion) and Br (brain) at PAE0, 4 and 8 indicated that Hex4, BBOX1, Lsd1, FMO, Tf and JHBP are extremely highly expressed in both the FB and FLT (Fig. 2D, Fig. S2). The verification of high-expression of these 6 genes can potentially identify the unknown tissue as a fat body-like tissue.

3.3. Morphological and cytological features of the FB and FLT

Although both the FB and FLT belong to the perivisceral fat body/fat body-like tissue based on their location in the hemocoel (Arrese and Soulages, 2010), the FLT shows dramatic structural differences with the

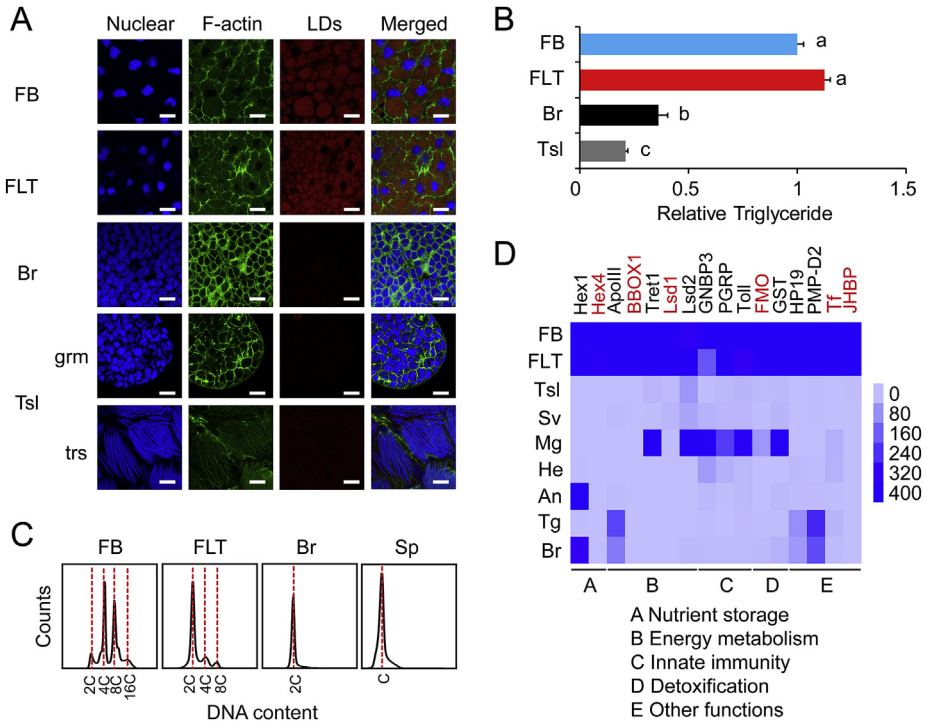

Fig. 2. Characteristics of the FB and FLT compared to other tissues in male locusts at PAE8. (A) Lipid droplets in the FB, FLT, Br and Tsl. LDs, lipid droplets. Nuclei were stained with Hoechst 33342 (blue), F-actin were stained with Phalloidin-Alexa Fluor 488 (green) and lipid droplets were stained with Nile red (red). Br, Brain; Tsl, testis follicles; grm, germinative area; trs, zone of transformation. Scale bar, 50 μm. (B) Relative triglyceride in the FB, FLT, Br and Tsl. n = 6. (C) Flow cytometry analysis of DNA contents in the FB, FLT, Br and Sp. Sp, Sperm. (D) qRT-PCR verification of candidate marker genes in 9 representative tissues at PAE8. n = 4–6. Sv, seminal vesicle; Mg, midgut; He, hemolymph; An, antenna; Tg, thoracic ganglion; Br, brain. Hex1, hexamerin-like protein 1; Hex4, hexamerin-like protein 4; ApoIII, apolipophorin-III; BBOX1, gamma-butyrobetaine dioxygenase; Tret1, facilitated trehalose transporter Tret1; Lsd1, lipid storage droplets surface-binding protein 1; Lsd2, lipid storage droplets surface-binding protein 2; GNBP3, glucan recognition protein 3; PGRP, peptidoglycan recognition protein; FMO, Flavin-containing monooxygenase; GST, glutathione S-transferase omega; HP19, basic 19 kDa hemolymph protein; PMP-D2, PARS intercerebralis major peptide D2; Tf, transferrin; JHBP, juvenile hormone binding protein. (For interpretation of the references to colour in this figure legend, the reader is referred to the Web version of this article.)

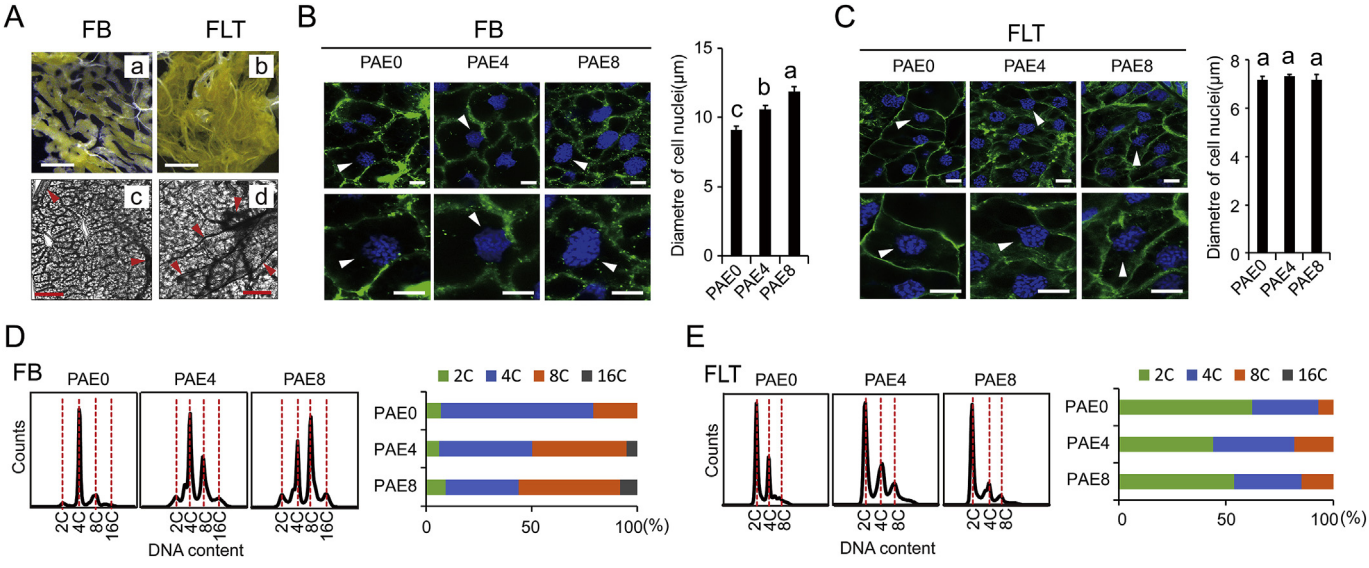

Fig. 3. Morphological and cytological features of FB and FLT cells in male locusts. (A) The tissue morphology of the FB and FLT at PAE8. Red arrow heads indicate tracheae. Scale bars: a and b, 500 μm; c and d, 50 μm. (B) The FB cell ploidy and nucleic diameter. (C) The FLT cell ploidy and nucleic diameter. Nuclei were stained with Hoechst 33342 (blue) and F-actin stained with Phalloidin-Alexa Fluor 488 (green). White arrow heads indicate nuclei. Lower panel is partially enlarged images of upper panel. Scale bar, 10 μm. (D) Flow cytometry analysis of DNA contents in the FB. (E) Flow cytometry analysis of DNA contents in the FLT. (For interpretation of the references to colour in this figure legend, the reader is referred to the Web version of this article.)

FB by comparing their morphology (Fig. 3A). The unfolded FB displays mesh shape (Fig. 3A, a), while the FLT cannot be unfolded and appears as compact mass (Fig. 3A and b). Moreover, only a few tracheae are distributed in the FB (Fig. 3A, c), whereas rich networks of tracheae in the FLT (Fig. 3A, d).

To further investigate the cytological characteristics of the FB and FLT, F-actin and nuclei were stained and imaged by confocal microscopy. Images showed that during adult maturation, nuclei of FB cells became larger and the diameter of cell nuclei increased from 9.14 μm at PAE0 to 11.91 μm at PAE8, while the size of FLT cells nuclei remain almost unchanged (Fig. 3B and C). Quantitative analysis of ploidy by flow cytometry showed that the FB had 4C peaks at PAE0, 4C peaks and 8C populations at PAE4, 8C peaks and 4C populations at PAE8 (Fig. 3D), while FLT cells were all maintained chiefly 2C peaks at PAE0, PAE4 and PAE8 (Fig. 3E).

3.4. Identification of specific genes in the FB and FLT

We performed the RNA-seq analysis to investigate the gene expression profiles of the FB and FLT at PAE0, PAE4 and PAE8. Principal component analysis (PCA) of 12 transcriptomic data (16753 genes in each transcriptomic data) indicated the cumulative proportion of PC1,

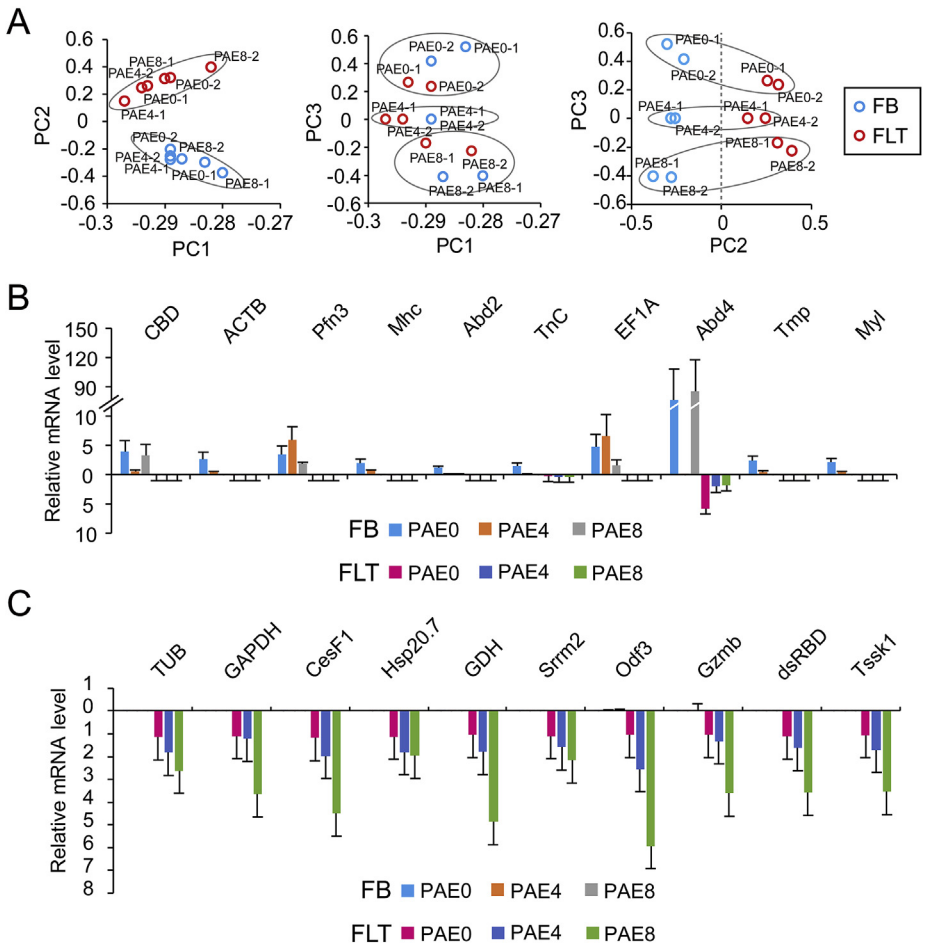

Fig. 4. Identification of specifically expressed genes in the FB or FLT. (A) Principal component analysis (PCA) of the transcriptomic data in the FB and FLT at PAE0, 4 and 8. (B) qRT-PCR verification of the top 10 specifically expressed genes in the FB at PAE0, 4 and 8. (C) qRT-PCR verification of the top 10 specifically expressed genes in the FLT at PAE0, 4 and 8.

PC2 and PC3 are totally 96.7% (Fig. 4A). As indicated by PC1 (89.5%), most genes have a similar expression pattern in both the FB and FLT. PC2 (5.8%) can obviously distinguish between the FB and FLT (Fig. 4A). PC3 (1.4%) can separate variant developmental stages (Fig. 4A).

To identify the specific genes to differentiate the two tissues, top 10 genes were selected as candidates according to the rank of absolute PC2 value in the FB and FLT, respectively (Fig. S3 A and B). qRT-PCR results confirmed that chitin binding domain (CBD), beta-actin (ACTB), profilin-1B (Pfn), myosin heavy chain isoform I (MhcI), insect cuticle protein (Abd2), troponin C (TnC), elongation factor 1A (EF1A), endocuticle structural glycoprotein ABD-4-like (Abd4), tropomyosin-1 (Tmp) and myosin light chain alkali (Myl) are highly expressed in the FB (Fig. 4B, Fig. S3 C). In the FLT, tubulin alpha-1B chain (TUB), glyceraldehyde-3-phosphate dehydrogenase 2 (GAPDH), carboxylesterase (CesF1), heat shock protein 20.7 (Hsp20.7), glutamate dehydrogenase (GDH), serine/arginine repetitive matrix protein 2-like (Srrm2), outer dense fiber protein 3 (Odf3), granzyme B (Gzmb), double-stranded RNA-binding domain (dsRBD) and testis-specific serine/threonine-protein kinase 1 (Tssk1) are highly expressed (Fig. 4C, Fig. S3 D).

3.5. Comparison of gene expression profiles between the FB and FLT

We firstly investigated the overall differentially expressed genes (DEGs) between the FB and FLT irrespective of the developmental stages by pooling PAE0, 4, 8-FB or PAE0, 4, 8-FLT together, respectively. Totally, 763 genes were up-regulated in the FB and 2624 genes were up-regulated in the FLT (Fig. 5A). The DEGs were further enriched by Kyoto Encyclopedia of Genes and Genomes (KEGG) pathway, Gene ontology (GO) and Interpro (IPR) analysis. The KEGG enrichment analysis showed that 5 pathways were up-regulated in the FB including Non-alcoholic fatty liver disease (NAFLD) (map04932), Oxidative phosphorylation (map00190), Alzheimer's disease (map05010), Parkinson's disease (map05012) and Huntington's disease (map05016) (Fig. 5B). Thirteen pathways were up-regulated in the FLT included cell cycle (map04110), progesterone-mediated oocyte maturation (map04914), ubiquitin mediated proteolysis (map04120), oocyte meiosis (map04114) and mismatch repair (map03430) (Fig. 5B). The GO enrichment analysis also indicated that genes of oxidation-reduction process were enriched in the FB, while genes of cell cycle and DNA metabolic process were enriched in the FLT (Table S2). The IPR enrichment analysis showed that zinc finger C2H2-like (IPR015880) was the most enriched item in the FLT and no enriched item in the FB (Table 1). Among these zinc finger C2H2-like genes, 99.12% genes belong to zinc finger transcriptional factors, which include the most altered 5 genes: transcriptional repressor scratch 1, zinc finger protein 135, RE1-silencing transcription factor, fez family zinc finger protein 1, zinc finger and SCAN domain-containing protein 32 (Table S3).

We then compared the DEGs between the FB and FLT at the same developmental stages. At PAE0, PAE4 and PAE8, 414, 269 and 1267 genes were up-regulated and 1371, 616 and 2278 genes were down-regulated respectively in the FB compared to FLT (Fig. 5C). Compare to PAE0 and PAE4, PAE8 displayed the most DEGs between the FB and FLT. The DEGs were enriched by KEGG pathway, GO and IPR analysis.

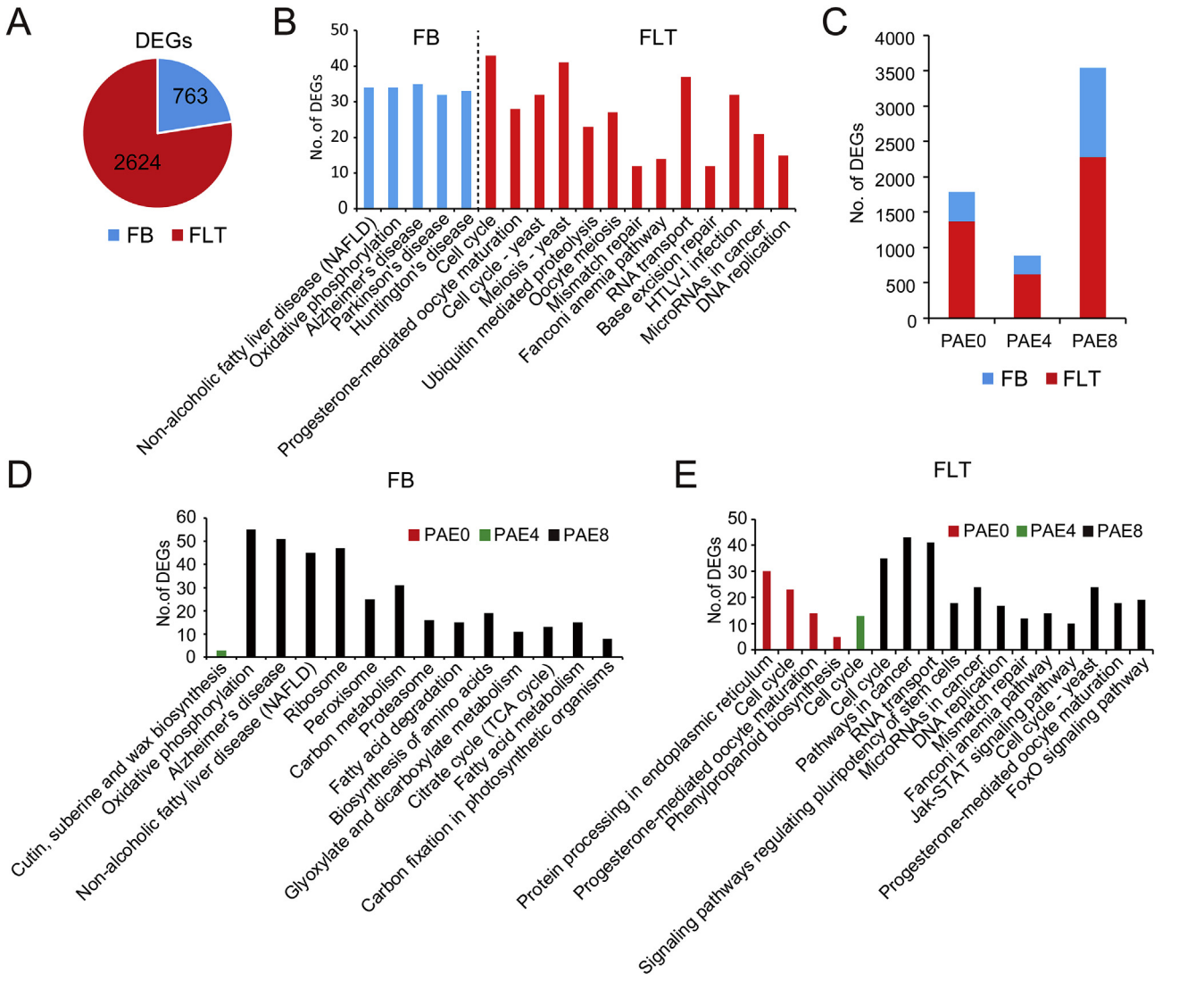

Fig. 5. Comparison of the differentially expressed genes (DEGs) between the FB and FLT. (A) Numbers of DEGs in the FB or FLT. (B) Enriched KEGG pathways in the FB or FLT. (C) Numbers of DEGs in the FB or FLT at PAE0, 4 and 8. (D) Enriched KEGG pathways in the FB. (E) Enriched KEGG pathways in the FLT.

Thirteen KEGG pathways were enriched in the FB at PAE8, which include energy metabolism related pathways such as oxidative phosphorylation (map00190), peroxisome (map04146), carbon metabolism (map01200), glyoxylate and dicarboxylate metabolism (map00630), citrate cycle (TCA cycle) (map00020), fatty acid degradation (map01212), as well as protein synthesis related pathways such as ribosome (map03010), proteasome (map03050) and biosynthesis of amino acids (map01230) (Fig. 5D). Twelve KEGG pathways were enriched in the FLT at PAE8, which include cell cycle (map04110), RNA transport (map03013), DNA replication (map03030), mismatch repair (map03430), progesterone-mediated oocyte maturation (map04914), Jak-STAT signaling pathway (map04630) and FoxO signaling pathway (map04068) (Fig. 5E). The GO and IPR enrichment analyses also indicated that genes of metabolic and biosynthetic process were enriched

Table 1
Enriched IPR items in the FLT or FB, respectively.

	IPR Id	IPR Title	Number of DEGs	Number of genes in Geneset	Qvalue
FLT	IPR015880	Zinc finger, C2H2-like	113	275	1.21E-15
	IPR026983	Dynein heavy chain	21	26	2.11E-11
	IPR016024	Armadillo-type fold	79	236	6.70E-05
	IPR001357	BRCT domain	12	18	3.42E-03
	IPR013083	Zinc finger, RING/FYVE/PHD-type	56	171	4.44E-03
	IPR004344	Tubulin-tyrosine ligase/Tubulin polyglutamylase	8	10	9.48E-03
	IPR009071	High mobility group box domain	14	27	9.96E-03
	IPR000048	IQ motif, EF-hand binding site	15	30	1.01E-02
	IPR000008	C2 domain	26	67	1.78E-02
	IPR001494	Importin-beta, N-terminal domain	8	11	2.12E-02
	IPR011009	Protein kinase-like domain	84	296	2.12E-02
FB					

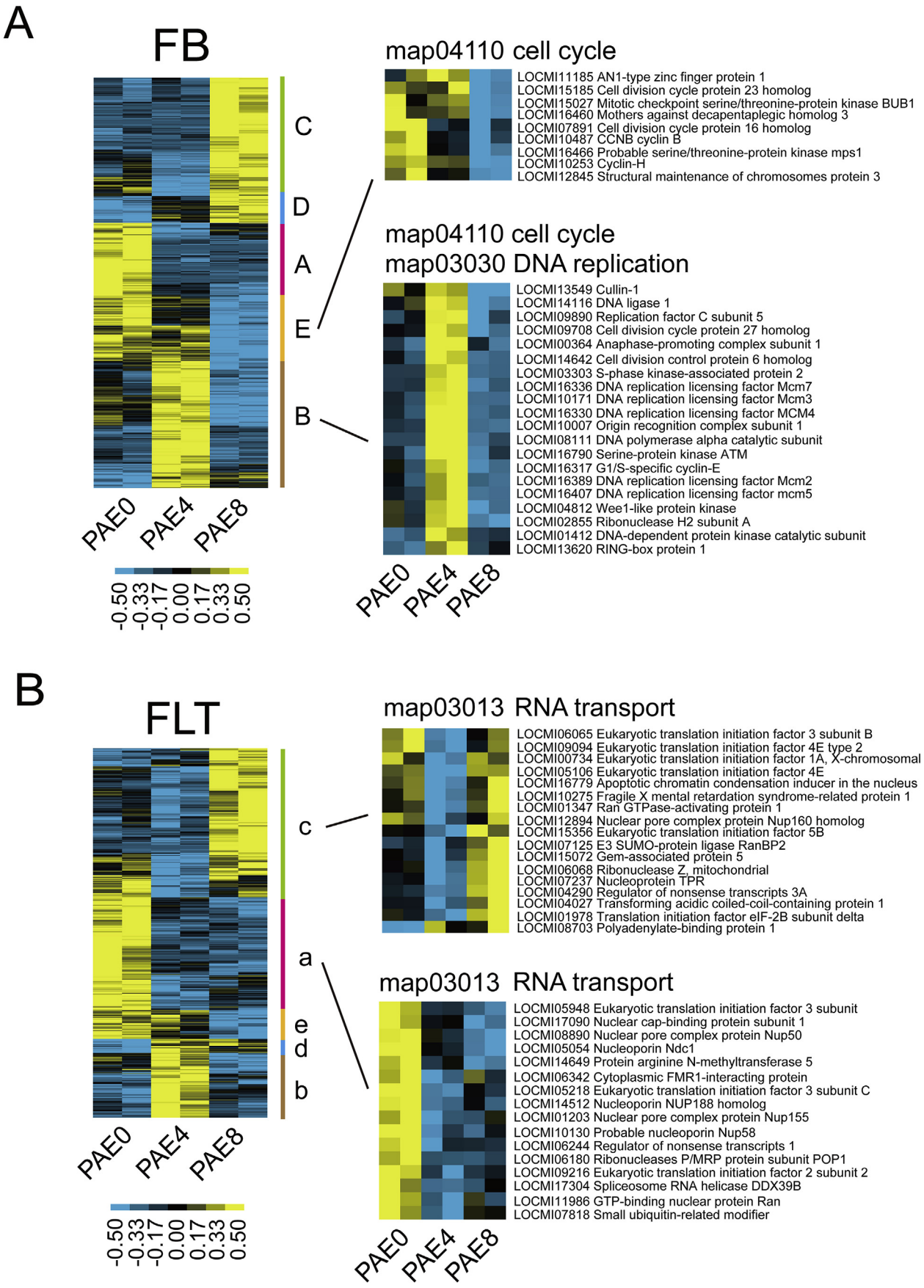

Fig. 6. The gene expression pattern in the FB or FLT during adult maturation in male locusts. (A) Cluster analysis of DEGs and KEGG pathway analysis of genes in each cluster in the FB at PAE0, 4 and 8. (B) Cluster analysis of DEGs and KEGG pathway analysis of genes in each cluster in the FLT at PAE0, 4 and 8.

in the FB, while genes of DNA metabolic process and cell cycle were enriched in the FLT (Table S4, Table S5).

3.6. Gene expression profiles of DEGs in the FB or FLT during the adult male maturation

During the adult male maturation from PAE0 to PAE8, 2543 and 2186 genes were differentially expressed in the FB and FLT, respectively, by the analysis of variance (ANOVA) (Fig. S4). To characterize the expression pattern of these DEGs, we further categorized the 2543 and 2186 DEGs by cluster analysis, respectively. In both the FB and FLT, the DEGs can be categorized into 5 clusters according to the gene expression profiles. Cluster A and a indicate highly expressed genes at PAE0. Cluster B and b indicate highly expressed genes at PAE4. Cluster C and c indicate highly expressed genes at PAE8. Cluster D and d indicate increasingly expressed genes. Cluster E and e indicate decreasingly expressed genes (Fig. 6A and B).

Although cluster A and a, cluster B and b, cluster C and c, cluster D and d, and cluster E and e have similar expression patterns, respectively, the enriched KEGG pathways are mostly different (Table S6, Fig. 6). In the FB, seven pathways were significantly enriched in Cluster A, twenty pathways were significantly enriched in Cluster B, eight pathways were significantly enriched in Cluster C, fourteen pathways were significantly enriched in Cluster D and seventeen pathways were significantly enriched in Cluster E (Table S6). The representative pathways in the FB were cell cycle (map04110) in cluster D and E, and DNA replication (map03030) in cluster E (Fig. 6A). DNA synthesis related genes, such as Mcm2 (mini-chromosome maintenance 2), Mcm3, Mcm4, Mcm5, Mcm7, DNA ligase1, cell division cycle protein 27, cell division control protein 6, G1/S-specific cyclin-E and S-phase kinase-associated protein 2 were highly expressed at PAE4 in cluster E (Fig. 6A). However, the genes for cell division, such as cell division cycle protein 23, cell division cycle protein 16, cyclin B, cyclin H and mitotic checkpoint serine/threonine-protein kinase BUB1, were increasingly downregulated from PAE0 to PAE8 in the FB (Fig. 6A).

In the FLT, KEGG analysis showed that fourteen pathways were significantly enriched in Cluster a, twenty pathways were significantly enriched in Cluster b, fifteen pathways were significantly enriched in Cluster c, no pathway was significantly enriched in Cluster d and nine pathways were significantly enriched in Cluster e (Table S6). The representative pathway was RNA transport (map03013) in cluster a and c. In cluster a, most genes were nuclear pore complex component proteins, such as nuclear cap-binding protein, nucleoporin Ndc1, nucleoporin Nup50, Nup188, Nup155 and Nup58. In cluster c, most genes were related to translation initiation, such as eIF1A (eukaryotic translation initiation factor 1A), eIF2B, eIF3B, eIF4E and eIF5B, were highly expressed at PAE8 (Fig. 6B).

3.7. Deficiency of spermatogenesis in testis follicles by FLT-deprivation

The testes were located in the abdominal cavity from the first segment to the forth segment (Fig. 7A). To investigate whether the FLT functions on the spermatogenesis in testis follicles, we deprived the FLT by operation. In the operation, the septum between the first and the second segment was cut open and the testes were pulled out (Fig. 7A and B). For the FLT-deprivation locust, the FLT was deprived from about 1/3 of all testis follicles using forceps and then the testes were put back (Fig. 7B). For the sham-operated locust, the testes were exposed the same time span in the air as the FLT-deprived locust and then put back without FLT-deprivation. The survival rate of operated locusts is 88.2% compared to 100% of sham-operated individuals (Fig. 7C). After 8 days post operation, the testis follicles in the operated area still remain uncovered by the FLT (Fig. 7D). FLT-deprived testis follicles displayed distortion in morphology and did not produce sperm bundles, in one of which includes thousands of mature sperms (Fig. 7D).

We further estimated the total sperm number in paired seminal vesicles of operated and sham-operated locusts at PAE10. FLT-deprivation significantly decreased the total sperm number by 38.8% (Fig. 7E). Among all sperms, 23.0% were dead sperms in the operated locusts compared to only 11.1% dead sperms in the sham-operated locusts (Fig. 7F).

4. Discussion

In this study, we identified a specialized fat body-like tissue adhering to testis follicles of male locusts, which have dramatic differences in morphology, cytology and transcriptome profiles. Fat bodies in the hemocoel were considered regionally differentiated, mainly displaying differences in trachea number, cellular mitochondria size and storage proteins granules abundance (Shirk and Malone, 1989; Wang and Haunerland, 1991). Regionally differentiated peripheral and perivisceral fat body cells are reported at the same level of polyploidy (Haunerland et al., 1990). We found that the FLT displayed divergence not only in the tissue structure but also in cell ploidy, especially the high ratio of diploid cells compared with the polyploidy cells of abdominal fat body (FB).

The FLT and FB showed differential gene expression profiles besides the differences in morphological and cytological characteristics. PCA analysis of transcriptomic data indicated that FB- or FLT-high expression genes are determined by their attached tissue types. Adhere to the cuticle and muscle, the FB expressed chitin binding domain (CBD), insect cuticle protein (Abd2) and endocuticle structural glycoprotein (Abd4), which are supposed to interact with extracellular chitin (Arakane et al., 2003; Zhao et al., 2017), and the FB also expressed troponin C (TnC) and tropomyosin-1 (Tmp), which are major components of muscle fibers (Andruchov and Galler, 2008; Crockford et al., 1991). Meanwhile, the FLT expressed genes that related to the development and maintenance of microenvironment during testis maturation. Outer dense fiber protein 3 (Odf3) specifically transcribed in spermatids to encode a coiled-coil protein of sperm tail outer dense fibers (Petersen et al., 2002). Heat shock protein 20.7 (Hsp20.7) and testis-specific serine/threonine-protein kinase 1 (Tssk1) have been reported highly expressed in the testis (Kou et al., 2016; MacLeod et al., 2014). The high expression of testis genes in the FLT might indicate a cross-effect between tissues (Roberts and Hebbard, 2016; Stanford and Goodyear, 2018). Carboxylesterases (CesF1) and Granzyme B (Gzmb) can response to cytotoxic molecules, suggesting the FLT's protection on the Tsl from exogenous toxins (Feng et al., 2018; Motyka et al., 2000). Besides, Serine/arginine repetitive matrix protein 2-like (Srrm2) and double-stranded RNA-binding domain (dsRBD) are involved in the RNA transport process to mediate faithful splicing of specific pre-mRNAs and RNAs localization (Schweisguth et al., 1994; Zanini et al., 2017). Accordingly, the most active pathway during the FLT development is RNA transport (Map 03013, Fig. 6B), indicating FLT cells underwent active RNA metabolism to prepare for protein synthesis during testis follicles maturation. In addition, genes of zinc finger C2H2-like (IPR015880) were the most enriched item and 99.12% genes belongs to zinc finger transcriptional factors. This suggested that complicated regulatory networks of gene expression were governed by zinc finger transcriptional factors in the FLT (Brayer and Segal, 2008). The FLT-deprivation operation further indicated that the FLT is indispensable for normal spermatogenesis in testis follicles. FLT cells are suggested to have a nutritional role during spermatogenesis (Bhakthan et al., 1969). In our study, considering the FLT penetrated between testis follicles and adhere to them tightly, we inferred that the FLT might also supply structural support for testis follicles, which is similar to Leydig cells in mammalians (Chen et al., 2017).

Fat body cells go through endocycle to form polyploidy cells for large scale protein synthesis during both larvae and adult stages (Guo et al., 2014; Smith and Orr-Weaver, 1991; Wu et al., 2016, 2018). All the 83 genes in cell cycle pathway (map 04110) were picked out from the transcriptome data based on the KEGG annotation. Among these

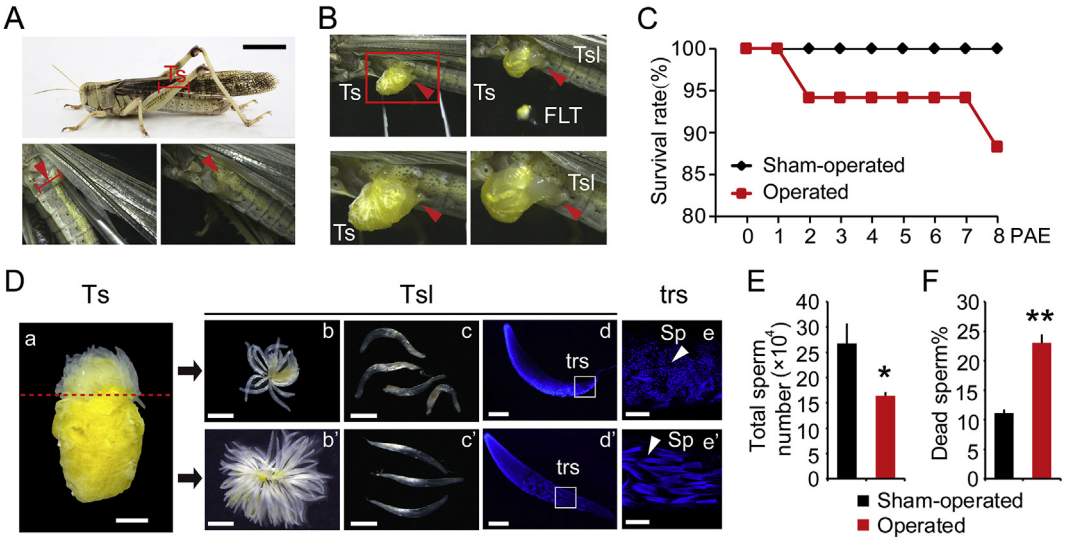

Fig. 7. FLT-deprivation operation of male locusts. (A) Operated site on the abdomen. Scale bar: 1 cm. (B) Partial FLT-deprivation by surgical operation at PAE0. Red arrowhead indicates operated part of the testes. (C) Survival rate of the sham-operated and operated locusts at PAE8. (D) Images of the Ts and Tsl in post-operated locusts at PAE8. (a) tissue above the red line, FLT-deprived Tsl; tissue below the red line, Tsl with FLT. (b and b') Tsl cluster. (c and c') single Tsl. (d and d') images of Tsl with nucleic staining. (e and e') zoomed images of trs. trs, zone of transformation; Sp, sperm. Scale bars: a, b and b', 2 mm; c and c', 1 mm; d and d', 200 μm; e and e', 100 μm. (E) Total sperm number in paired seminal vesicles of sham-operated and operated locusts at PAE10. (F) Percentage of dead sperm in paired seminal vesicles of sham-operated and operated locusts at PAE10. n = 6. *, $P < 0.05$ and **, $P < 0.01$. (For interpretation of the references to colour in this figure legend, the reader is referred to the Web version of this article.)

genes, 30 genes showed significant difference during adult maturation in the FB by ANOVA (Table S7). The up-regulated DNA synthesis genes and down-regulated cell division genes indicated that DNA replication were enhanced while G2/M switch were reduced, thus cell polyploidy is generated in the FB (Fig. S5). Unlike in the FB, only 15 genes in the cell cycle pathway showed significant difference in the FLT during the adult male maturation (Fig. S6, Table S7). However, when comparing the RPKM values of cell cycle genes between FLT and FB at PAE0, 4 and 8 respectively, the RPKM values of most genes are significantly higher in the FLT than in the FB (Table S7), suggesting that more FLT cells probably undergo a complete cell cycle rather than endocycle. Therefore, this could be the cause that most of FLT cells remain diploid, while FB cells were polyploid.

The two similar tissues undergo different cell cycle process at the same developmental stage, and mitotic markers genes Cyclin A and Cyclin B as well as the mitotic-related pathway Foxo signaling pathway were altered in the FLT (Deng et al., 2001; Jouandin et al., 2014). These special characteristics implicate that the two kinds of tissues could be used as a novel model for MES (mitotic/endocycle switch) study. Mammalian trophoblast giant cells and megakaryocyte, *Arabidopsis* trichome cells, and *Drosophila* follicle cells have been used in exploring the regulatory mechanism of MES. In human placenta, subgroups of trophoblast cells enter the endocycle and terminally differentiate to become trophoblast giant cells, but the signals that triggers the endocycle transition is unknown (Swanson et al., 2015). Megakaryocytes undergo endomitosis, and the transition from mitotic to endomitotic cycle is influenced by the secreted thrombopoietin (Swanson et al., 2015). In *Arabidopsis*, the transition from the mitotic cycle to the endocycle is modulated by Auxin (Ishida et al., 2009). Among those models, the follicle cells in the *Drosophila* ovary seems to be the most well studied system to the mitotic-to-endocycle transition. *Drosophila* follicle cells undergo multiple rounds of mitotic divisions until mid-oogenesis (stage 6) and then uniformly switch from the normal mitotic cycle and enter the endocycle (Royzman and Orr-Weaver, 1998). Previous study indicated that the transition from mitotic cycles to endocycles should be developmentally programmed (Ishida et al., 2009). Thus, it is hard to clearly discriminate which genes are directly involved in MES regulation (Deng et al., 2001). Besides, MES regulation may vary in different cell types. Notch gene controls the switches of different cell cycle programs in follicle cells, yet the nurse cell endocycles are normal in Notch mutant clones (Lilly and Duronio, 2005). Therefore, the FB-FLT tissues in locusts offer a novel model system to study MES, which can avoid the disturbances of developmental signals.

Interestingly, plenty of genes were enriched in pathways in cancer (map 05200) and signaling pathways regulating pluripotency of stem cells (map 04550) in the FLT of locusts. Pathways in cancer includes several crucial pathways. Genes in PI3K-Akt signaling pathway, mTOR signaling pathway, Ras signaling pathway, FoxO signaling pathway and Wnt signaling pathway were activated. However, genes in p53 signaling pathway and MAPK signaling pathway were inactive. p53 has pivotal functions in cell cycle progression, as it regulates G1/S, S, and G2/M cell cycle checkpoints (Giono and Manfredi, 2006). The inactivation of p53 signaling pathway suggested its roles on the continuous proliferation of FLT cells. In the signaling pathways regulating pluripotency of stem cells, three epigenetic regulators were highly expressed. SMARCAD1 (SWI/SNF-related matrix-associated actin-dependent regulator of chromatin subfamily A containing DEAD/H) plays a direct role in DNA end resection and recombinational DNA double-strand break repair (Costelloe et al., 2012). Eggless/SETDB1 (Histone-lysine N-methyltransferase) is required for controlling germline stem cell maintenance and differentiation (Wang et al., 2011). Jarid2 (Protein Jumonji) regulates proliferation and differentiation of cardiomyocytes (Nakajima et al., 2011; Shirato et al., 2009). Epigenetic regulation plays critical roles in cell proliferation, fate determination, survival and self-renewal and lineage differentiation of embryonic stem cells (Jiang et al., 2019; Wang et al., 2011). Therefore, the activation of epigenetic regulators in the FLT indicated its communication with the Tsl, which could also be considered as an evidence that the expression of some genes in the fat body may depend on its attached tissue types.

In summary, we identified a specialized fat body-like tissue that is critical for spermatogenesis in testis follicles of locust. This fat body-like tissue undergoes mainly mitotic cell cycle instead of endocycle; thus, the cells were mostly diploid during the development. Besides, the two similar tissues are functionally differentiated and have respective gene expression patterns. These differences in the two tissues made them a potential model to study the mechanism of MES.

Author contributions

L. Kang, W. Guo and D. Ren designed the research; D. Ren, J Song, L. Zhao performed the research; D. Ren, W. Guo, P. Yang and J. He analyzed data; and L. Kang, W. Guo and D. Ren wrote the paper.

Acknowledgments

This work was supported by National Natural Science Foundation of China grants (31572333 and 31771452), Strategic Priority Research Program of the Chinese Academy of Sciences (XDB11010200), and the Youth Innovation Promotion Association, CAS (No. 2016080).

Appendix A. Supplementary data

Supplementary data to this article can be found online at https://doi.org/10.1016/j.ibmb.2019.103207.

References

Anders, S., Pyl, P.T., Huber, W., 2015. HTSeq-a Python framework to work with high-throughput sequencing data. Bioinformatics 31, 166–169.
Andruchov, O., Galler, S., 2008. Influence of fast and slow alkali myosin light chain isoforms on the kinetics of stretch-induced force transients of fast-twitch type IIA fibres of rat. Pflügers Archiv 455, 1165–1172.
Arakane, Y., Zhu, Q.S., Matsumiya, M., Muthukrishnan, S., Kramer, K.J., 2003. Properties of catalytic, linker and chitin-binding domains of insect chitinase. Insect Biochem. Mol. Biol. 33, 631–648.
Arrese, E.L., Soulages, J.L., 2010. Insect fat body: energy, metabolism, and regulation. Annu. Rev. Entomol. 55, 207–225.
Beissbarth, T., Speed, T.P., 2004. GOstat: find statistically overrepresented Gene Ontologies within a group of genes. Bioinformatics 20, 1464–1465.
Bhakthan, N.M.G., Nair, K.K., Borden, J.H., 1969. Occorrence of a fat body layer around the testes of ips confusus (Coleoptera:Scolytidae). Scientific notes 62, 1495–1496.
Boigegrain, R.A., Mattras, H., Brehélin, M., Paroutaud, P., Coletti-Previero, M.A., 1992. Insect immunity: two proteinase inhibitors from hemolymph of *Locusta migratoria*. Biochem. Biophys. Res. Commun. 189, 790–793.
Bramsiepe, J., Wester, K., Weinl, C., Roodbarkelari, F., Kasili, R., Larkin, J.C., Hulskamp, M., Schnittger, A., 2010. Endoreplication controls cell fate maintenance. PLoS Genet. 6 e1000996.
Brayer, K.J., Segal, D.J., 2008. Keep your fingers off my DNA: protein-protein interactions mediated by C2H2 zinc finger domains. Cell Biochem. Biophys. 50, 111–131.
Chandrasekar, R., Jae, S.S., Krishnan, M., 2008. Expression and localization of storage protein 1 (SP1) in differentiated fat body tissues of red hairy caterpillar, *Amsacta albistriga* Walker. Arch. Insect Biochem. Physiol. 69, 70–84.
Chen, H., Wang, Y., Ge, R., Zirkin, B.R., 2017. Leydig cell stem cells: identification, proliferation and differentiation. Mol. Cell. Endocrinol. 445, 65–73.
Costelloe, T., Louge, R., Tomimatsu, N., Mukherjee, B., Martini, E., Khadaroo, B., Dubois, K., Wiegant, W.W., Thierry, A., Burma, S., van Attikum, H., Llorente, B., 2012. The yeast Fun30 and human SMARCAD1 chromatin remodellers promote DNA end resection. Nature 489, 581–584.
Crockford, T., Wommack, K.E., Johnston, I.A., McAndrew, B.J., Mutungi, G., Johnson, T.P., 1991. Inter- and intra-specific variation in myosin light chain and troponin I composition in fast muscle fibres from two species of fish (genus Oreochromis) which have different temperature-dependent contractile properties. J. Muscle Res. Cell Motil. 12, 439–446.
Damiens, D., Bressac, C., Brillard, J.P., Chevrier, C., 2002. Qualitative aspects of sperm stock in males and females from *Eupelmus orientails* and *Dinarmus basalis* (Hymenoptera: chalcidoidea) as revealed by dual fluorescence. Physiol. Entomol. 27, 97–102.
de Oliveira, V.T.P., da Cruz-Landim, C., 2003. Morphology and function of insect fat body cells: a review. BIOCIÊNCIAS, Porto Alegre 11, 195–205.
Deng, W.M., Althauser, C., Ruohola-Baker, H., 2001. Notch-Delta signaling induces a transition from mitotic cell cycle to endocycle in *Drosophila* follicle cells. Development 128, 4737–4746.
Dortland, J.F., Esch, T.H., 1979. A fine structural survey of the development of the adult fat body of *Leptinotarsa decemlineata*. Cell Tissue Res. 201, 423–430.
Feng, X., Li, M., Liu, N., 2018. Carboxylesterase genes in pyrethroid resistant house flies, *Musca domestica*. Insect Biochem. Mol. Biol. 92, 30–39.
Giono, L.E., Manfredi, J.J., 2006. The p53 tumor suppressor participates in multiple cell cycle checkpoints. J. Cell. Physiol. 209, 13–20.
Guo, W., Wu, Z., Song, J., Jiang, F., Wang, Z., Deng, S., Walker, V.K., Zhou, S., 2014. Juvenile hormone-receptor complex acts on Mcm4 and Mcm7 to promote polyploidy and vitellogenesis in the migratory locust. PLoS Genet. 10, e1004702.
Guo, W., Wu, Z., Yang, L., Cai, Z., Zhao, L., Zhou, S., 2019. Juvenile hormone-dependent Kazal-type serine protease inhibitor Greglin safeguards insect vitellogenesis and egg production. FASEB J. 33, 917–927.
Haunerland, N.H., 1995. Regional and functional differentiation in the insect fat body. Annu. Rev. Entomol. 40, 121–145.
Haunerland, N.H., Nair, K.K., Bowers, W.S., 1990. Fat body heterogeneity during development of *Heliothis zea*. Insect Biochem. 20, 829–837.
Inze, D., De Veylder, L., 2006. Cell cycle regulation in plant development. Annu. Rev. Genet. 40, 77–105.
Ishida, T., Adachi, S., Yoshimura, M., Shimizu, K., Umeda, M., Sugimoto, K., 2009. Auxin modulates the transition from the mitotic cycle to the endocycle in *Arabidopsis*. Development 137, 63–71.
Jiang, F., Liu, Q., Liu, X., Wang, X.H., Kang, L., 2019. Genomic data from arthropods reveal high conservation but divergent evolutionary pattern of Polycomb/Trithorax group genes in arthropods. Insect Sci. 26, 20–34.
Jordan, K.C., Schaeffer, V., Fischer, K.A., Gray, E.E., Ruohola-Baker, H., 2006. Notch signaling through tramtrack bypasses the mitosis promoting activity of the JNK pathway in the mitotic-to-endocycle transition of *Drosophila* follicle cells. BMC Dev. Biol. 6, 16.
Jouandin, P., Ghiglione, C., Noselli, S., 2014. Starvation induces FoxO-dependent mitotic-to-endocycle switch pausing during *Drosophila* oogenesis. Development 141, 3013–3021.
Kim, D., Pertea, G., Trapnell, C., Pimentel, H., Kelley, R., Salzberg, S.L., 2013. TopHat2: accurate alignment of transcriptomes in the presence of insertions, deletions and gene fusions. Genome Biol. 14, R36.
Kou, L.H., Wu, H.H., Liu, Y.M., Zhang, Y.P., Zhang, J.Z., Guo, Y.P., Ma, E.B., 2016. Molecular characterization of six small heat shock proteins and their responses under cadmium stress in *Oxya chinensis* (Orthoptera: acridoidea). Environ. Entomol. 45, 258–267.
Levy, F., Bulet, P., Ehret-Sabatier, L., 2004. Proteomic analysis of the systemic immune response of *Drosophila*. Mol. Cell. Proteom. 3, 156–166.
Li, S., Yu, X., Feng, Q., 2019. Fat body biology in the last decade. Annu. Rev. Entomol. 64, 315–333.
Lilly, M.A., Duronio, R.J., 2005. New insights into cell cycle control from the *Drosophila* endocycle. Oncogene 24, 2765–2775.
MacLeod, G., Shang, P., Booth, G.T., Mastropaolo, L.A., Manafpoursakha, N., Vogl, A.W., Varmuza, S., 2014. PPP1CC2 can form a kinase/phosphatase complex with the testis-specific proteins TSSK1 and TSKS in the mouse testis. Reproduction 147, 1–12.
Motyka, B., Korbutt, G., Pinkoski, M.J., Heibein, J.A., Caputo, A., Hobman, M., Barry, M., Shostak, I., Sawchuk, T., Holmes, C.F.B., Gauldie, J., Bleackley, R.C., 2000. Mannose 6-phosphate/insulin-like growth factor II receptor is a death receptor for Granzyme B during cytotoxic T cell–induced apoptosis. Cell 103, 491–500.
Nakajima, K., Inagawa, M., Uchida, C., Okada, K., Tane, S., Kojima, M., Kubota, M., Noda, M., Ogawa, S., Shirato, H., Sato, M., Suzuki-Migishima, R., Hino, T., Satoh, Y., Kitagawa, M., Takeuchi, T., 2011. Coordinated regulation of differentiation and proliferation of embryonic cardiomyocytes by a jumonji (Jarid2)-cyclin D1 pathway. Development 138, 1771–1782.
Palm, W., Sampaio, J.L., Brankatschk, M., Carvalho, M., Mahmoud, A., Shevchenko, A., Eaton, S., 2012. Lipoproteins in *Drosophila melanogaster*-assembly, function, and influence on tissue lipid composition. PLoS Genet. 8, e1002828.
Petersen, C., Aumuller, G., Bahrammi, M., Hoyer-fender, S., 2002. Molecular cloning of Odf3 encoding a novel coiled-coil protein of sperm tail outer dense fibers. Mol. Reprod. Dev. 61, 102–112.
Ren, D., Cai, Z., Song, J., Wu, Z., Zhou, S., 2014. dsRNA uptake and persistence account for tissue-dependent susceptibility to RNA interference in the migratory locust, *Locusta migratoria*. Insect Mol. Biol. 23, 175–184.
Rizki, T.M., Rizki, R.M., 1972. Developmental biology and genetics of adipose tissue of the Drosophila larva. Egypt. J. Genet. Cytol. 1, 173–188.
Roberts, A.A., Hebbard, L.W., 2016. Molecular cross-talk between the liver and white adipose tissue links excessive noURIshment to hepatocellular carcinoma. Transl. Cancer Res. 5, 1222–1226.
Robinson, M.D., Oshlack, A., 2010. A scaling normalization method for differential expression analysis of RNA-seq data. Genome Biol. 11, R25.
Royzman, I., Orr-Weaver, T.L., 1998. S phase and differential DNA replication during *Drosophila* oogenesis. Genes Cells 3, 767–776.
Schweisguth, D.C., Chelladurai, B.S., Nicholsonl, A.W., Moore, P.B., 1994. Structural characterization of a ribonuclease III processing signal. Nucleic Acids Res. 22, 604–612.
Shirato, H., Ogawa, S., Nakajima, K., Inagawa, M., Kojima, M., Tachibana, M., Shinkai, Y., Takeuchi, T., 2009. A jumonji (Jarid2) protein complex represses cyclin D1 expression by methylation of histone H3-K9. J. Biol. Chem. 284, 733–739.
Shirk, P.D., Malone, C.C., 1989. Regional differentiation of fat bodies in larvae of the indianmeal moth, *Plodia interpunctella*. Arch. Insect Biochem. Physiol. 12, 187–199.
Smith, A.V., Orr-Weaver, T.L., 1991. The regulation of the cell cycle during *Drosophila* embryogenesis: the transition to polyteny. Development 112, 997–1008.
Stanford, K.I., Goodyear, L.J., 2018. Muscle-adipose tissue cross talk. Cold Spring Harb Perspect Med 8.
Swanson, C.I., Meserve, J.H., McCarter, P.C., Thieme, A., Mathew, T., Elston, T.C., Duronio, R.J., 2015. Expression of an S phase-stabilized version of the CDK inhibitor Dacapo can alter endoreplication. Development 142, 4288–4298.
Szollosi, A., Marcaillou, C., 1977. Electron microscope study of the blood-testis barrier in an insect: *Locusta migratoria*. J. Ultrastruct. Res. 59, 158–172.
Szollosi, A., Marcaillou, C., 1979. The apical cell of the locust testis: an ultrastructural study. J. Ultrastruct. Res. 69, 331–342.
Tysell, B., Butterworth, F.M., 1978. Different rate of protein granule formation in the larval fat body of *Drosophila melanogaster*. J. Insect Physiol. 24, 201–206.
Vanishree, V., Nirmala, X., Arul, E., Krishnan, M., 2005. Differential sequestration of storage proteins by various fat body tissues during post-larval development in silkworm, *Bombyx moriL*. Invertebr. Reprod. Dev. 48, 81–88.
Wang, X., Fang, X., Yang, P., Jiang, X., Jiang, F., Zhao, D., Li, B., Cui, F., Wei, J., Ma, C., Wang, Y., He, J., Luo, Y., Wang, Z., Guo, X., Guo, W., Wang, X., Zhang, Y., Yang, M., Hao, S., Chen, B., Ma, Z., Yu, D., Xiong, Z., Zhu, Y., Fan, D., Han, L., Wang, B., Chen,

Y., Wang, J., Yang, L., Zhao, W., Feng, Y., Chen, G., Lian, J., Li, Q., Huang, Z., Yao, X., Lv, N., Zhang, G., Li, Y., Wang, J., Wang, J., Zhu, B., Kang, L., 2014. The locust genome provides insight into swarm formation and long-distance flight. Nat. Commun. 5, 2957.

Wang, X., Pan, L., Wang, S., Zhou, J., McDowell, W., Park, J., Haug, J., Staehling, K., Tang, H., Xie, T., 2011. Histone H3K9 trimethylase Eggless controls germline stem cell maintenance and differentiation. PLoS Genet. 7, e1002426.

Wang, Y., Yang, P., Cui, F., Kang, L., 2013. Altered immunity in crowded locust reduced fungal (Metarhizium anisopliae) pathogenesis. PLoS Pathog. 9, e1003102.

Wang, Z., Haunerland, N.H., 1991. Ultrastructural study of storage protein granules in fat body of the corn earworm, *Heliothis zea*. J. Insect Physiol. 37, 353–363.

Wu, Z., Guo, W., Xie, Y., Zhou, S., 2016. Juvenile hormone activates the transcription of Cell-division-cycle 6 (Cdc6) for polyploidy-dependent insect vitellogenesis and oogenesis. J. Biol. Chem. 291, 5418–5427.

Wu, Z., Guo, W., Yang, L., He, Q., Zhou, S., 2018. Juvenile hormone promotes locust fat body cell polyploidization and vitellogenesis by activating the transcription of Cdk6 and E2f1. Insect Biochem. Mol. Biol. 102, 1–10.

Yang, P., Hou, L., Wang, X., Kang, L., 2019. Core transcriptional signatures of phase change in the migratory locust. Protein Cell. https://doi.org/10.1007/s13238-019-0648-6.

Zanini, I.M., Soneson, C., Lorenzi, L.E., Azzalin, C.M., 2017. Human cactin interacts with DHX8 and SRRM2 to assure efficient pre-mRNA splicing and sister chromatid cohesion. J. Cell Sci. 130, 767–778.

Zhao, X., Gou, X., Qin, Z., Li, D., Wang, Y., Ma, E., Li, S., Zhang, J., 2017. Identification and expression of cuticular protein genes based on *Locusta migratoria* transcriptome. Sci. Rep. 7, 45462.